Femtosecond time-resolved five-wave mixing at silicon surfaces

2005 J. Phys.: Condens. Matter 17 S221

(http://iopscience.iop.org/0953-8984/17/8/003)

INSTITUTE OF PHYSICS PUBLISHING JOURNAL OF PHYSICS: CONDENSED MATTER

J. Phys.: Condens. Matter **17** (2005) S221–S244 doi:10.1088/0953-8984/17/8/003

Femtosecond time-resolved five-wave mixing at silicon surfaces

T Meier, M Reichelt, S W Koch and U Höfer

Department of Physics and Material Sciences Centre, Philipps University, Renthof 5, D-35032 Marburg, Germany

Received 16 June 2004, in final form 11 October 2004
Published 11 February 2005
Online at stacks.iop.org/JPhysCM/17/S221

Abstract

The ultrafast dynamics of photoexcitations at silicon surfaces is investigated using a surface-sensitive purely optical technique. In the experiments, the diffracted second harmonic generated by sequences of ultrashort laser pulses is detected as a function of the time delay between the pulses. It is demonstrated that this five-wave-mixing technique can be used to measure the temporal evolution of the optical polarization and the photoexcited populations at the surface. The experimental results can be reproduced by numerical solutions of optical Bloch equations. The theoretical analysis allows one to investigate which dephasing times and relaxation processes are compatible with experiment. Furthermore, it is outlined how one can describe optical nonlinearities at surfaces using a microscopic theory within the framework of semiconductor Bloch equations.

(Some figures in this article are in colour only in the electronic version)

1. Introduction

Optical techniques have been used successfully to obtain important information on the dynamics of excited states in atoms, molecules, and condensed matter systems. In particular, for semiconductor systems time-resolved nonlinear optical spectroscopy using short laser pulses has provided valuable insight into the temporal evolution of particles and quasi-particles in non-equilibrium situations [1–4]. Two techniques which are well established for investigating the coherent dynamics of bulk systems and heterostructures are four-wave mixing (4WM) and pump–probe spectroscopy. Depending on the particular set-up, these techniques can be used to monitor the temporal evolution of photoexcited polarizations and populations [1–4].

The detailed mechanisms of carrier scattering and recombination at surfaces and interfaces are not only of fundamental interest but their control is also critical for the performance of modern small scale devices. However, compared to that of bulk and quantum well structures, the electron dynamics at semiconductor surfaces and interfaces is currently not well understood. At present, most of the experimental information on the dynamics of electronic excitations at

surfaces has been obtained by means of time-resolved two-photon photoemission (2PPE). This powerful technique can be used to determine energy and parallel momentum of intermediate states, i.e., to study the dynamics of photoexcited populations in k-space [5–16]. However, 2PPE measurements are generally restricted to conducting surfaces in ultrahigh vacuum environments. In particular, the small escape depth of photoelectrons does not normally permit one to access buried interfaces. In the case of semiconductor or insulator surfaces band bending or charging induced by the pump pulses can severely limit the resolution.

In this paper, we describe a surface-sensitive time-resolved technique that is complementary to the 2PPE one and review recent experimental results which have been obtained at silicon surfaces. The method combines 4WM with second-harmonic generation (SHG). SHG is dipole forbidden in the bulk of centrosymmetric materials and has become a very successful all-optical probe of surfaces and interfaces [17, 18]. The combination of 4WM and SHG results in a five-wave-mixing (5WM) process. As in 4WM, in the 5WM set-up the material is excited by a number of laser pulses originating from different directions and the field emitted in a background-free diffraction direction is detected. However, unlike in ordinary 4WM, the signal measured in 5WM is not detected at a similar frequency to those of the incident laser beams but instead the intensity of the second-harmonic (SH) radiation is recorded. The generation of the FWM signal can be viewed as the scattering of SHG from a transient excitation grating which has been generated by two laser beams. By inducing a transient grating with ultrashort laser pulses and analysing the diffracted SH intensity the method yields considerably more information than conventional pump and SHG probe experiments [19, 20]. In particular, it is possible to access the ultrafast coherent regime at surfaces in a conceptually straightforward way just like using 4WM in the bulk [21, 22]. As an optical probe 5WM is applicable not only to most surfaces but also to the interfaces between many different materials.

For a description of the basic physics of the type of nonlinear processes in general and transient grating techniques such as 4WM and 5WM in particular, let us consider that surface and the near-surface region of a solid excited by two laser beams with frequencies ω_a and ω_b which propagate in the directions $\mathbf{k}_a$ and $\mathbf{k}_b$, respectively. In linear optics, i.e., in first order in the incident field, part of each of these beams is reflected giving rise to fields of frequencies ω_a and ω_b which are emitted in the directions corresponding to the dashed lines in figure 1(a). If the intensity of the incident radiation is sufficiently high the material gives rise to a nonlinear response and additional fields appear which are of higher order in the incident beams. From non-centrosymmetric systems, such as a surface, one gets a finite optical response in second order in the field. For example, if only a single beam a (b) is incident one can measure SHG, i.e., an emitted field that oscillates with $2\omega_a$ ($2\omega_b$) and propagates in the reflection direction of beam a (b). For the case where the system is excited by two beams, the nonlinear optical material will mix the excitations induced by the individual beams which gives rise to sum-frequency generation (SFG), i.e., a field that oscillates with frequency $\omega_a + \omega_b$ and that is emitted in direction $\mathbf{K}_{\mathrm{SF}}$ with $K_{\mathrm{SF},x} = k_{a,x} + k_{b,x}$ if the surface is in the x–z plane; see figure 1(a). The physical origin of these second-order signals is two interactions between the material and the light field inducing optical polarizations in the material which oscillate with the sum of the frequencies.

In third order in the incident field, one may generally have two different kinds of optical nonlinearities. On the one hand, it is possible to additively mix the frequencies of the beams and to generate fields with frequencies $3\omega_a$, $3\omega_b$, $2\omega_a + \omega_b$, and $\omega_a + 2\omega_b$ that are emitted in directions $3k_{a,x}$, $3k_{b,x}$, $2k_{a,x} + k_{b,x}$, and $k_{a,x} + 2k_{b,x}$, respectively. Such third-order sum-frequency generation processes will, however, not be considered in the following. On the other hand, third-order optical interactions also give rise to fields with frequencies ω_a, ω_b, $2\omega_a - \omega_b$, and $-\omega_a + 2\omega_b$ that are emitted in directions $k_{a,x}$, $k_{b,x}$, $2k_{a,x} - k_{b,x}$, and $-k_{a,x} + 2k_{b,x}$,

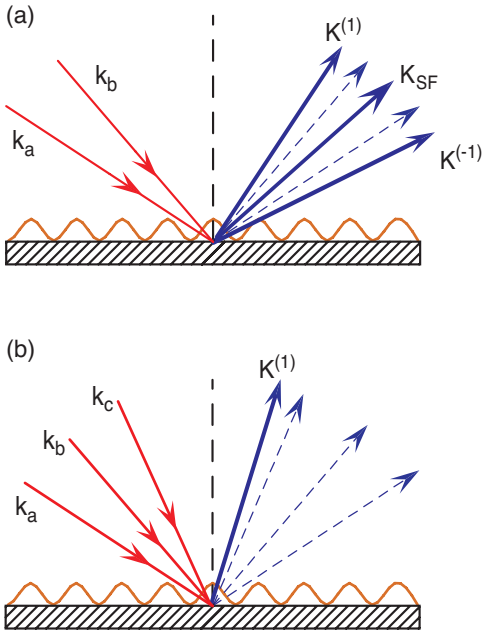

Figure 1. A schematic drawing of wave-mixing processes at surfaces in reflection geometry; (a) for two and (b) for three incident laser beams, respectively. Further explanation is given in the text.

respectively. The latter two fields are self-diffracted 4WM signals which like the SFG propagate in directions which involve both pulses. One can, for example, write the direction of the last diffracted signal as $k_{b,x} + (k_{b,x} - k_{a,x})$. Here, $k_{b,x} - k_{a,x}$ corresponds to a population grating which is produced in second order by the combined action of beams a and b. This population grating is modulated spatially according to $\cos(k_G x)$, with $k_G = k_{b,x} - k_{a,x}$; see figure 1(a). The self-diffracted 4WM signal is due to that part of beam b that is scattered off the population grating into the signal direction $k_{b,x} + (k_{b,x} - k_{a,x})$. By measuring the intensity of such 4WM signals as a function of the time delay between beams a and b one may obtain information on the decay (dephasing) of the material polarization induced by the first beam a.

The 4WM process is not surface specific. On the contrary, 4WM is frequently used to measure dephasing in bulk semiconductors and semiconductor nanostructures, such as quantum wells, where the diffracted signal is usually measured in transmission. In a reflection geometry, as indicated in figure 1(a), the typical probing depth of the 4WM signal is 10–30 nm. Such experiments are capable of monitoring the carrier dynamics *near* a surface but do not achieve true surface specificity [23, 24]. In order to yield specific information about the carrier dynamics in the topmost 1–3 atomic layers where the electronic structure differs from that of the bulk, the nonlinear process should be symmetry forbidden in the volume but allowed at the surface. In the case of centrosymmetric materials this requirement is fulfilled by all processes that are of even order in the applied field.

In this paper, we focus on analysing a surface specific nonlinear optical response which is of fourth order in the incident beams. In some of the experimental results, the intensity of the (SH) radiation is measured in the diffraction direction $\mathbf{K}^{(1)}$ with $K_x^{(1)} = 3k_{b,x} - k_{a,x} = 2k_{b,x} + (k_{b,x} - k_{a,x})$; see figure 1(a). As a generalization of the 4WM process this signal can be understood considering that beam b is frequency doubled and scattered off the population grating induced by beams a and b. As in ordinary 4WM, one can therefore expect that by measuring the intensity of the diffracted (SH) radiation as a function of the time delay between beams a and b, one can gain information on the dephasing of the polarization induced by beam a.

Other experimental results presented in this paper have been obtained using three incident beams a, b, and c. In this set-up, the intensity of the SH radiation is measured in the diffraction direction $\mathbf{K}^{(1)}$ with $K_x^{(1)} = 2k_{c,x} + (k_{b,x} - k_{a,x})$; see figure 1(b). Thus, beam c is frequency doubled and scattered off the population grating induced by beams a and b. As outlined below, in the three-beam experiments all time delays between the incident pulses can be varied independently, which allows one to measure not only dephasing of polarizations but also the dynamics of the population grating.

Results obtained with this technique are presented and discussed for two Si surfaces. At the Si(111)7 × 7 surface, the self-diffracted SH intensity is measured as a function of the time delay between the two incident ultrashort laser beams. As discussed in section 4, the time-delay dependence of this signal reflects the dynamics of the optical polarization induced by the pump beam [21]. On the basis of the experimental transients alone one cannot decide whether the observed ultrafast dynamics is due to the decay of individual uncoupled polarizations, i.e., a T_2 process, or whether it is the result of the destructive interference of a system of coupled polarizations. As demonstrated by numerical solutions of the optical Bloch equations (OBE) for two model systems, a microscopic modelling of the SHG including all relevant optical matrix elements and further interaction processes is required, if one wants to distinguish between these processes.

At the Si(001)-c(4 × 2) surface, the diffracted SH intensity is measured as a function of the time delays between three incident ultrashort laser beams. As discussed in section 5, by varying individual time delays between the three pulses one can not only investigate the dynamics of one-photon transitions but also follow the temporal evolution of populations and two-photon transitions. With the support of model calculations based on the OBE the measured ultrafast response as a function of a particular delay can be assigned to the scattering of the excited electrons within the D_{down} surface band on timescales of 50–500 fs [22].

Before presenting and discussing the experimental results on the dynamics of the diffracted SHG in sections 4 and 5, we summarize in section 3 some information on the experimental set-up. Our theoretical approaches for analysing the ultrafast coherent nonlinear optical response of surfaces are discussed in section 2. A microscopic theory which is capable of describing the dynamics of nonlinear optical surface excitations [25, 26] is presented in section 2.1. This approach combines *ab initio* calculations of the band structure performed including quasiparticle corrections within the GW method [27–29] with the semiconductor Bloch equations (SBE), which have been used successfully for the analysis of the nonlinear optical response of bulk semiconductors and semiconductor heterostructures [1–4]. Although this is, in principle, straightforward, the microscopic approach has not yet been extended and applied to study surface-sensitive experiments such as SHG, 2PPE, and 5WM ones. Therefore, in section 2.2 we describe how ultrafast SHG can be analysed using phenomenological sets of OBE. Solutions of the OBE for a number of model systems are compared to experimental data on two-beam and three-beam 5WM in sections 4 and 5. This comparison demonstrates that for a more detailed understanding of the dynamical processes which govern nonlinear optical experiments at surfaces, analysis with an adequate microscopic theory would be very beneficial.

2. Theory

In our theoretical modelling of the transient optical response of surface excitations we use two different approaches. In the more phenomenological one—see section 2.2—we make assumptions about the states which dominate the optical response and calculate the signals by considering all populations and coherences among these states within the framework of OBE which were originally developed for analysing the optical response of atomic systems [30].

In this approach, the energies of the states, their coupling to the light field, and the dephasing and relaxation times are regarded as parameters which are chosen to get the best agreement with the experimental data. Such phenomenological descriptions have been used frequently, e.g., to analyse optical transients in semiconductor heterostructures; see [31–33] where biexciton contributions to 4WM have been investigated. This method which is used in sections 4 and 5 to analyse two-beam and three-beam 5WM experiments is described in section 2.2.

As a problem of the phenomenological OBE approach, one should keep in mind that the fitting parameters are often not uniquely determined, but their validity may depend on the experimental conditions. As shown, e.g., in [34], a particular set of parameters which is able to fit differential absorption spectra of a semiconductor heterostructure for resonant excitonic excitation may fail if one analyses off-resonant configurations, such as in the optical Stark effect. Consequently, this type of approach does not have general predictive capabilities, since one may have to adjust parameters if the excitation conditions are varied.

Not only for these reasons it is preferable if one can use a microscopic theory which relies only on a few well known material parameters to describe the optical response. Such microscopic approaches have been developed for many semiconductors and semiconductor heterostructures. The dynamics of optical excitations in such systems can often be described rather accurately at the level of SBE [4]. These equations go well beyond the OBE by including many-body interactions which give rise to excitonic resonances, Coulomb correlations, carrier–carrier and carrier–phonon scattering, and more.

Due to the added complexity, any analysis at the level of SBE is considerable more complicated than a phenomenological description. However, one reduces in this way the need for phenomenological parameters and the theory gains predictive capabilities. Ideally, one can use the microscopic theory to predict signals for many different experimental conditions without having to adjust any material parameters. An adequate microscopic theory is also able to describe the decay of the optical polarization and the relevant carrier relaxation processes [3, 4, 35–39].

So far, time-resolved SHG at surfaces has not been treated on a fully microscopic level. However, nonlinear optical signals of the excitonic resonance at the Si(111)-(2 × 1) surface have been computed using the SBE [25, 26]. Here, the dispersions and wavefunctions of the relevant bands were obtained from density functional theory with quasiparticle correction. This procedure and a few results are briefly described in section 2.1.

2.1. Semiconductor Bloch equations for the nonlinear optical response of surface excitons

As presented in [25, 26], the following microscopic Hamiltonian can be used to analyse the exciton resonance of the Si(111)-(2 × 1) surface:

$$H = H_0 + H_{\mathrm{C}} + H_{\mathrm{l-m}}. \tag{1}$$

Here, H_0 contains the single-particle energies, i.e., the band structure, and $H_{\mathrm{l-m}}$ accounts for the coupling between a classical light field and the material system. H_{C} describes the mutual Coulomb interaction between the photoexcited carriers. This term extends the current analysis beyond the description presented in section 2.2.

The band structure part of the Hamiltonian is given by

$$H_0 = \sum_{\mathbf{k}} E^{\mathrm{c}}_{\mathbf{k}} c^{\dagger}_{\mathbf{k}} c_{\mathbf{k}} + \sum_{\mathbf{k}} E^{\mathrm{v}}_{\mathbf{k}} d^{\dagger}_{-\mathbf{k}} d_{-\mathbf{k}}, \tag{2}$$

where $E^{\mathrm{v}}_{\mathbf{k}}$ ($E^{\mathrm{c}}_{\mathbf{k}}$) is the dispersion of the valence (conduction) band, $d^{\dagger}_{\mathbf{k}}$ ($c^{\dagger}_{\mathbf{k}}$) is a hole (electron) creation operator, and $d_{\mathbf{k}}$ ($c_{\mathbf{k}}$) denotes the corresponding annihilation operator. The subscript $\mathbf{k}$ is the wavevector.

At the level of the dipole approximation, the light–matter interaction is given by

$$H_{\mathrm{l-m}} = -\mathbf{E}(t)\cdot\mathbf{P} = -\mathbf{E}(t)\cdot\left[\sum_{\mathbf{k}}(\boldsymbol{\mu}_{\mathbf{k}}^{cd}c_{\mathbf{k}}^{\dagger}d_{-\mathbf{k}}^{\dagger} + (\boldsymbol{\mu}_{\mathbf{k}}^{cd})^{*}d_{-\mathbf{k}}c_{\mathbf{k}})\right], \tag{3}$$

where $\boldsymbol{\mu}_{\mathbf{k}}^{cd}$ is the dipole matrix element for the interband transition at wavevector $\mathbf{k}$. In equation (3), $\mathbf{P}$ is the macroscopic optical interband polarization which is defined by the sum in the square bracket, i.e., by adding up all electron–hole transitions multiplied by the interband dipole matrix element.

The many-body Coulomb interaction consists of several terms which describe the repulsion of equally charged carriers, the attraction between electrons and holes, and the exchange term

$$\begin{aligned} H_{\mathrm{C}} = {} & \tfrac{1}{2}\sum_{\mathbf{k}',\mathbf{p},\mathbf{q}} V^{cccc}_{\mathbf{k}'+\mathbf{q},\mathbf{p}-\mathbf{q},\mathbf{p},\mathbf{k}'}c^{\dagger}_{\mathbf{k}'+\mathbf{q}}c^{\dagger}_{\mathbf{p}-\mathbf{q}}c_{\mathbf{p}}c_{\mathbf{k}'} \\ & + \tfrac{1}{2}\sum_{\mathbf{k}',\mathbf{p},\mathbf{q}} V^{dddd}_{-\mathbf{k}',-\mathbf{p},-\mathbf{p}+\mathbf{q},-\mathbf{k}'-\mathbf{q}}d^{\dagger}_{\mathbf{k}'+\mathbf{q}}d^{\dagger}_{\mathbf{p}-\mathbf{q}}d_{\mathbf{p}}d_{\mathbf{k}'} \\ & - \sum_{\mathbf{k}',\mathbf{p},\mathbf{q}} V^{cddc}_{\mathbf{k}'+\mathbf{q},-\mathbf{p},-\mathbf{p}+\mathbf{q},\mathbf{k}'}c^{\dagger}_{\mathbf{k}'+\mathbf{q}}d^{\dagger}_{\mathbf{p}-\mathbf{q}}d_{\mathbf{p}}c_{\mathbf{k}'} \\ & - \sum_{\mathbf{k}',\mathbf{p},\mathbf{q}} V^{dcdc}_{-\mathbf{k}',\mathbf{k}'+\mathbf{q},\mathbf{q}-\mathbf{p},\mathbf{p}}c^{\dagger}_{\mathbf{k}'+\mathbf{q}}d^{\dagger}_{\mathbf{p}-\mathbf{q}}c_{\mathbf{p}}d_{\mathbf{k}'}, \end{aligned} \tag{4}$$

where $V^{l_1l_2l_3l_4}_{\mathbf{k}_1\mathbf{k}_2\mathbf{k}_3\mathbf{k}_4}$ denotes the Coulomb matrix element of four states [25].

In [25, 26], the energy dispersions appearing in equation (2) were taken from the quasiparticle band structure which has been obtained by *ab initio* many-body perturbation theory within the GW method [27–29]. The matrix elements that show up in equations (4) and (3) have been evaluated using the quasiparticle wavefunctions of the GW method. Thus all terms entering the Hamiltonian have been determined from microscopic *ab initio* many-body theory.

To calculate dynamical properties of the photoexcited system, we evaluate the Heisenberg equations of motion for the relevant microscopic quantities. Starting with the equation of motion for the interband transition $p_{\mathbf{k}} = \langle d_{-\mathbf{k}}c_{\mathbf{k}}\rangle$ we then have to face the well known hierarchy problem, since via the Coulomb interaction the two-point quantity $p_{\mathbf{k}}$ couples to four-point quantities (expectation values containing products of four operators); the four-point quantities couple to six-point quantities; etc [4]. As in [25, 26], we truncate the many-body hierarchy by applying the time-dependent Hartree–Fock approximation which leads to a closed set of equations at the two-point level. This means that besides $p_{\mathbf{k}}$ we have to consider the electron and hole densities $n_{\mathrm{c},\mathbf{k}} = \langle c^{\dagger}_{\mathbf{k}}c_{\mathbf{k}}\rangle$ and $n_{\mathrm{v},\mathbf{k}} = \langle d^{\dagger}_{-\mathbf{k}}d_{-\mathbf{k}}\rangle$, respectively [4, 40, 41]. Many-body correlations beyond the Hartree–Fock treatment, that have been studied, e.g., in [1–4, 42–45], are neglected here. These correlations are often crucial for configurations in which the Hartree–Fock contributions vanish, or more generally for any detailed quantitative description of realistic systems. However, the Hartree–Fock approach still yields qualitatively and almost quantitatively correct results for the optical Stark effect induced by a strongly detuned linearly polarized pump. This is due to the fact that the correlation contributions decay with a higher power of the inverse detuning than the Hartree–Fock terms [44].

The resulting coupled equations of motion for the interband transitions and the electron and hole populations, i.e., the SBE, are given by

$$\begin{aligned} \frac{\partial}{\partial t}p_{\mathbf{k}} = {} & -\frac{\mathrm{i}}{\hbar}(E^{\mathrm{c}}_{\mathbf{k}} + E^{\mathrm{v}}_{\mathbf{k}})p_{\mathbf{k}} + \frac{\mathrm{i}}{\hbar}(1 - n_{\mathrm{c},\mathbf{k}} - n_{\mathrm{v},\mathbf{k}})\left[\boldsymbol{\mu}^{cd}_{\mathbf{k}}\cdot\mathbf{E}(t) + \sum_{\mathbf{q}}(V^{cddc}_{\mathbf{k},\mathbf{q},\mathbf{k},\mathbf{q}} - V^{dcdc}_{\mathbf{q},\mathbf{k},\mathbf{k},\mathbf{q}})p_{\mathbf{q}}\right] \\ & + \frac{\mathrm{i}}{\hbar}p_{\mathbf{k}}\sum_{\mathbf{q}}(V^{cccc}_{\mathbf{k},\mathbf{q},\mathbf{k},\mathbf{q}}n_{\mathrm{c},\mathbf{q}} + V^{dddd}_{\mathbf{k},\mathbf{q},\mathbf{k},\mathbf{q}}n_{\mathrm{v},\mathbf{q}}) + \left.\frac{\partial p_{\mathbf{k}}}{\partial t}\right|_{\mathrm{corr}}, \end{aligned} \tag{5}$$

$$\frac{\partial}{\partial t} n_{\mathrm{c},\mathbf{k}} = \frac{\mathrm{i}}{\hbar}\mathbf{E}(t)\cdot(\boldsymbol{\mu}^{cd}_{\mathbf{k}} p^*_{\mathbf{k}} - \boldsymbol{\mu}^{cd*}_{\mathbf{k}} p_{\mathbf{k}}) + \frac{\mathrm{i}}{\hbar} p^*_{\mathbf{k}} \sum_{\mathbf{q}} (V^{cddc}_{\mathbf{k},\mathbf{q},\mathbf{k},\mathbf{q}} - V^{dcdc}_{\mathbf{q},\mathbf{k},\mathbf{k},\mathbf{q}}) p_{\mathbf{q}}$$
$$- \frac{\mathrm{i}}{\hbar} p_{\mathbf{k}} \sum_{\mathbf{q}} (V^{cddc}_{\mathbf{q},\mathbf{k},\mathbf{q},\mathbf{k}} - V^{dcdc}_{\mathbf{k},\mathbf{q},\mathbf{q},\mathbf{k}}) p^*_{\mathbf{q}} + \left.\frac{\partial n_{\mathrm{c},\mathbf{k}}}{\partial t}\right|_{\mathrm{corr}}, \tag{6}$$

$$\frac{\partial}{\partial t} n_{\mathrm{v},\mathbf{k}} = \frac{\mathrm{i}}{\hbar}\mathbf{E}(t)\cdot(\boldsymbol{\mu}^{cd}_{\mathbf{k}} p^*_{\mathbf{k}} - \boldsymbol{\mu}^{cd*}_{\mathbf{k}} p_{\mathbf{k}}) + \frac{\mathrm{i}}{\hbar} p^*_{\mathbf{k}} \sum_{\mathbf{q}} (V^{cddc}_{\mathbf{k},\mathbf{q},\mathbf{k},\mathbf{q}} - V^{dcdc}_{\mathbf{q},\mathbf{k},\mathbf{k},\mathbf{q}}) p_{\mathbf{q}}$$
$$- \frac{\mathrm{i}}{\hbar} p_{\mathbf{k}} \sum_{\mathbf{q}} (V^{cddc}_{\mathbf{q},\mathbf{k},\mathbf{q},\mathbf{k}} - V^{dcdc}_{\mathbf{k},\mathbf{q},\mathbf{q},\mathbf{k}}) p^*_{\mathbf{q}} + \left.\frac{\partial n_{\mathrm{v},\mathbf{k}}}{\partial t}\right|_{\mathrm{corr}}. \tag{7}$$

Note that compared to the equations presented in [4], the interband exchange interaction (the last line of equation (4)) has also been considered; it gives rise to the terms proportional to V^{dcdc} in equations (5)–(7). This term is known to be small for bulk semiconductors and heterostructures close to the fundamental direct band gap, but may be quantitatively important for surface excitations. The terms denoted by $\frac{\partial \cdots}{\partial t}|_{\mathrm{corr}}$ formally represent many-body correlations beyond the Hartree–Fock approximation, which give rise to, e.g., exciton populations, biexciton resonances, as well as dephasing and relaxation. In what follows, these terms are approximated by introducing a T_2 time modelling dephasing of the interband transitions and a T_1 time describing energy relaxation and scattering of populations.

As shown in [25], our method is able to reproduce the measured [46] and previously calculated [29] linear optical spectrum of the Si(111)-(2 × 1) surface. Since all matrix elements are evaluated using the wavefunctions obtained from *ab initio* calculations, our approach includes the strong optical anisotropy which is a result of the formation of Pandey chains [47]. In the linear spectra, the Coulomb interaction gives rise to a strongly absorbing exciton resonance which appears approximately 0.25 eV below the band gap [25]; see the solid curve in figure 2(b).

In the following we present results on pump-induced changes of the absorption spectra of the Si(111)-(2×1) surface, which were obtained by solving equations (5)–(7) numerically using 429 **k**-points. The dephasing time T_2 is chosen to model a phenomenological homogeneous broadening with a full width at half-maximum (FWHM) of 50 meV. In order to focus on the optical Stark effect, we monitor the change of the absorption when exciting the surface with a pump pulse well below the exciton resonance. To analyse these changes it is advantageous to consider the differential absorption spectrum, which is defined as [4]

$$\delta\alpha(\omega) = \alpha(\omega)|_{\text{with pump}} - \alpha(\omega)|_{\text{without pump}}. \tag{8}$$

In the numerical evaluation of the nonlinear absorption we solve equations (5)–(7) for the pump–probe geometry. The strong pump is treated nonperturbatively, whereas the probe is assumed to be weak and thus only included in first order [4].

The calculations are performed using a Gaussian-shaped pump pulse with a duration of 250 fs which is tuned to 0.3 eV. The 0.15 eV detuning to the surface exciton is bigger than the homogeneous linewidth and the spectral width of the pump pulse. The pumping therefore creates an off-resonant excitation of the system which temporally follows the envelope of the incident pulse. The spectra displayed in figure 2 are obtained assuming an ultrashort, i.e., spectrally white, probe pulse, which arrives at the temporal maximum of the pump. The predominantly dispersive shape of the differential absorption spectra with positive (negative) contributions on the high (low) energy side shown in figure 2(a) corresponds to a pump-intensity-dependent blue shift of the exciton resonance; see figure 2(b). This blue shift is a consequence of the coupling between the exciton and the pump field which causes a renormalization of the resonance energy which has its origin in the level repulsion of quantum

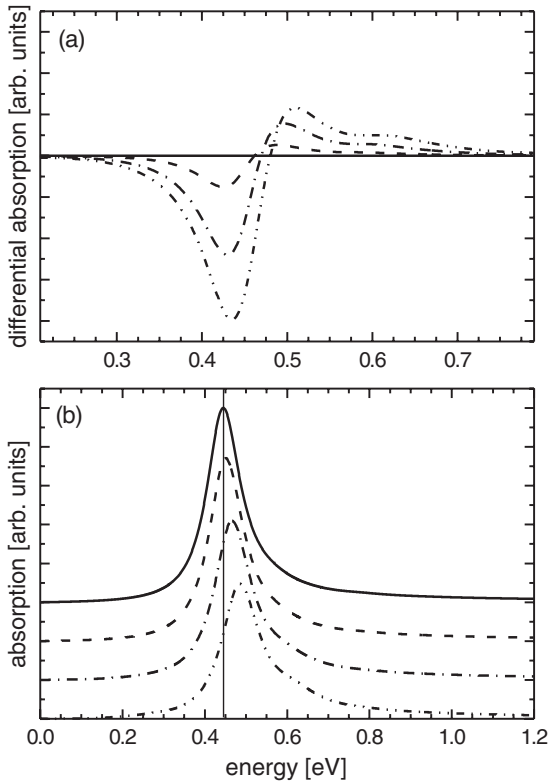

Figure 2. (a) Differential absorption spectra for different intensities of the pump pulse and (b) corresponding absorption spectra. The relative intensities are I_0 (dashed), $4I_0$ (dash–dotted) and $9I_0$ (dash–dot–dotted) respectively. The solid curve shows the linear spectrum. For better visibility the spectra in (b) are displaced vertically. Taken from [25].

mechanically coupled states. The Stark effect behaviour of the surface exciton resonance is analogous to that of a non-resonantly excited two level system and also similar to that of excitons in direct-gap semiconductor heterostructures [4, 42–44].

From figure 2(b), one can see that besides the blue shift with increasing pump intensity also the oscillator strength of the exciton peak is decreasing. This reduction of the absorption peak is mainly due to phase-space filling, i.e., the term proportional to $(1 - n_{\mathrm{c},\mathbf{k}} - n_{\mathrm{v},\mathbf{k}})$ in equation (5) [4, 42–44]. Since a pump pulse of higher intensity transiently generates more carriers in the system, it is clear that due to this term the absorption of the probe beam will be reduced, i.e., bleaching is observed. Additionally, to the blue shift and bleaching of the surface exciton, for higher pump intensity weak signatures from energetically higher exciton states start to show up in the differential absorption spectra; see the dash–dot–dotted curve in figure 2(a).

The theoretical approach described here and straightforward extensions should also be well suited for the analysis of other nonlinear and time-resolved optical experiments investigating surface properties, such as SHG and 2PPE ones. In the future, we plan to go beyond the time-dependent Hartree–Fock approximation used here and to solve the SBE including many-body correlations. This will enlarge the applicability of our approach and enable us to study relaxation and dephasing as well as interactions among surface excitons.

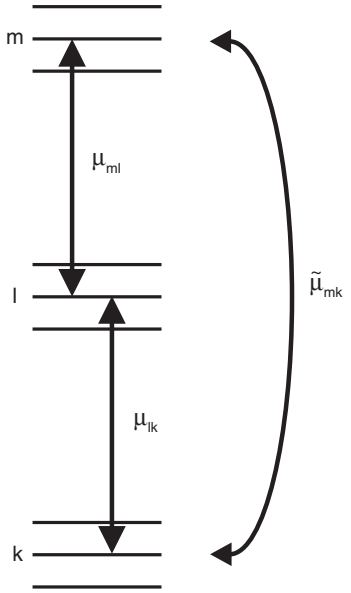

Figure 3. A schematic drawing of a three-band multi-level system. k labels the states of the lowest band, e.g., the initially occupied valence band. l and m denote the states of the intermediate (conduction) band and the highest band, respectively. The frequency of the exciting laser pulses is assumed to be close to the energy differences between states l and k as well as m and l. The optical excitation thus creates resonant interband transitions which are proportional the interband dipole matrix elements $\boldsymbol{\mu}_{lk}$ and $\boldsymbol{\mu}_{ml}$. Due to optical nonlinearities such an excitation generates coherences between the states m and k which oscillate with twice the excitation frequency and therefore give rise to SHG. The 2ω polarization is proportional to the matrix elements $\tilde{\boldsymbol{\mu}}_{mk}$.

2.2. Optical Bloch equations for second-harmonic generation

In SHG, one pulse creates a resonant polarization with frequency ω which is converted by a second pulse into a resonant polarization with frequency 2ω. Thus, any modelling requires at least three levels with dipole allowed optical transitions. Considering band to band transitions in solid-state systems, these levels should in fact be treated as bands which may be approximated by a densely spaced collection of states. Following these considerations we show in the following how the time-resolved SHG induced by sequences of ultrashort laser pulses can be analysed using a general three-band multi-level system; see figure 3.

The Hamiltonian which describes the temporal evolution of the photoexcited system consists of two terms:

$$H = H_0 + H_{\mathrm{l-m}}. \tag{9}$$

Here, H_0 is the material part which contains the energies of the states considered:

$$H_0 = \sum_k \epsilon_k c_k^\dagger c_k + \sum_l \epsilon_l c_l^\dagger c_l + \sum_m \epsilon_m c_m^\dagger c_m. \tag{10}$$

As shown in figure 3, the index k labels the states of the lowest (valence) band, l those of the intermediate (conduction) band, and m those of the highest band, respectively. $c_i^\dagger$ and c_i are creation and annihilation operators for state i. As long as many-body interactions are neglected one could just as well replace these operators by *kets* and *bras*, i.e., work within single-particle quantum mechanics [4, 48]. Here, however, we use the second-quantization operators to discuss the OBE in a similar way to the many-body particle systems in section 2.1.

In equation (9), $H_{\mathrm{l-m}}$ describes the interaction between a classical light field and the material system. In the dipole approximation it is given by

$$H_{\mathrm{l-m}} = -\mathbf{E}(t)\cdot\mathbf{P} = -\mathbf{E}(t)\cdot\left[\sum_{lk}(\boldsymbol{\mu}_{lk}c_l^\dagger c_k + \boldsymbol{\mu}_{lk}^* c_k^\dagger c_l) + \sum_{ml}(\boldsymbol{\mu}_{ml}c_m^\dagger c_l + \boldsymbol{\mu}_{ml}^* c_l^\dagger c_m) + \sum_{mk}(\tilde{\boldsymbol{\mu}}_{mk}c_m^\dagger c_k + \tilde{\boldsymbol{\mu}}_{mk}^* c_k^\dagger c_m)\right], \tag{11}$$

where $\mathbf{P}$, i.e., the term in the square brackets, is the total optical polarization of the material. Assuming that the transition energies satisfy $\epsilon_l - \epsilon_k \approx \epsilon_m - \epsilon_l \approx \hbar\omega$ implies that $\epsilon_m - \epsilon_k \approx 2\hbar\omega$. Therefore, the terms of the first two sums that contribute to the polarization oscillate in time, $\propto e^{\pm i\omega t}$, whereas the last term oscillates twice as fast, $\propto e^{\pm i2\omega t}$. This means that one can decompose the polarization into two contributions:

$$\mathbf{P} = \mathbf{P}_\omega + \tilde{\mathbf{P}}_{2\omega}, \tag{12}$$

with

$$\begin{aligned}\mathbf{P}_\omega &= \sum_{lk}(\boldsymbol{\mu}_{lk}c_l^\dagger c_k + \boldsymbol{\mu}_{lk}^* c_k^\dagger c_l) + \sum_{ml}(\boldsymbol{\mu}_{ml}c_m^\dagger c_l + \boldsymbol{\mu}_{ml}^* c_l^\dagger c_m),\\ \tilde{\mathbf{P}}_{2\omega} &= \sum_{mk}(\tilde{\boldsymbol{\mu}}_{mk}c_m^\dagger c_k + \tilde{\boldsymbol{\mu}}_{mk}^* c_k^\dagger c_m),\end{aligned} \tag{13}$$

where $\tilde{\mathbf{P}}_{2\omega}$ gives rise to the signals measured in SHG. In order to distinguish in the notation clearly between the ω and 2ω polarizations, the terms connected to the latter one are denoted by $\tilde{\mathbf{P}}$ and $\tilde{\boldsymbol{\mu}}$.

If the incident fields are spectrally centred close to the frequency ω, they will not directly produce $\tilde{\mathbf{P}}_{2\omega}$ since this contribution is way off resonance. Therefore, one can in this case concentrate on the resonant part of the light–matter interaction, i.e.,

$$H_{\mathrm{l-m}} = -\mathbf{E}(t)\cdot\mathbf{P}_\omega = -\mathbf{E}(t)\cdot\left[\sum_{lk}(\boldsymbol{\mu}_{lk}c_l^\dagger c_k + \boldsymbol{\mu}_{lk}^* c_k^\dagger c_l) + \sum_{ml}(\boldsymbol{\mu}_{ml}c_m^\dagger c_l + \boldsymbol{\mu}_{ml}^* c_l^\dagger c_m)\right]. \tag{14}$$

The dynamics of the photoexcited system is determined by the temporal evolution of all possible populations and coherences of the states considered. The expectation values of the relevant quantities are defined as

$$\begin{aligned} p_{lk} &= \langle c_l^\dagger c_k\rangle, \qquad p_{ml} = \langle c_m^\dagger c_l\rangle, \qquad \tilde{p}_{mk} = \langle c_m^\dagger c_k\rangle,\\ n_{kk'} &= \langle c_k^\dagger c_{k'}\rangle, \qquad n_{ll'} = \langle c_l^\dagger c_{l'}\rangle, \qquad \text{and} \qquad n_{mm'} = \langle c_m^\dagger c_{m'}\rangle.\end{aligned}$$

Here p_{ab} and $\tilde{p}_{ab}$ are interband coherences between the states a and b, whereas n_{ab} are either intraband coherences if $a \neq b$ or populations of the state a if $a = b$.

In order to obtain dynamical equations for the relevant expectation values, we use the Heisenberg equation,

$$\frac{\partial}{\partial t}\mathcal{O} = \frac{\mathrm{i}}{\hbar}[H, \mathcal{O}], \tag{15}$$

written here for the general operator $\mathcal{O}$. Inserting the operator combinations introduced above, evaluating the commutators with the Hamiltonian H, and taking expectation values, we obtain the following equations:

$$\frac{\partial}{\partial t}p_{lk} = -\frac{\mathrm{i}}{\hbar}(\epsilon_k - \epsilon_l)p_{lk} - \frac{\mathrm{i}}{\hbar}\mathbf{E}(t)\cdot\sum_{k'}\boldsymbol{\mu}_{lk'}^* n_{k'k} + \frac{\mathrm{i}}{\hbar}\mathbf{E}(t)\cdot\sum_{l'}\boldsymbol{\mu}_{l'k}^* n_{ll'} - \frac{\mathrm{i}}{\hbar}\mathbf{E}(t)\cdot\sum_{m'}\boldsymbol{\mu}_{m'l}\tilde{p}_{m'k}, \tag{16}$$

$$\frac{\partial}{\partial t}\, p_{ml} = -\frac{\mathrm{i}}{\hbar}(\epsilon_l - \epsilon_m)\, p_{ml} - \frac{\mathrm{i}}{\hbar}\mathbf{E}(t)\cdot\sum_{l'}\boldsymbol{\mu}^*_{ml'} n_{l'l} + \frac{\mathrm{i}}{\hbar}\mathbf{E}(t)\cdot\sum_{m'}\boldsymbol{\mu}^*_{m'l} n_{mm'} + \frac{\mathrm{i}}{\hbar}\mathbf{E}(t)\cdot\sum_{k'}\boldsymbol{\mu}_{lk'}\tilde{p}_{mk'}, \tag{17}$$

$$\frac{\partial}{\partial t}\,\tilde{p}_{mk} = -\frac{\mathrm{i}}{\hbar}(\epsilon_k - \epsilon_m)\,\tilde{p}_{mk} - \frac{\mathrm{i}}{\hbar}\mathbf{E}(t)\cdot\sum_{l'}\boldsymbol{\mu}^*_{ml'} p_{l'k} + \frac{\mathrm{i}}{\hbar}\mathbf{E}(t)\cdot\sum_{l'}\boldsymbol{\mu}^*_{l'k} p_{ml'}, \tag{18}$$

$$\frac{\partial}{\partial t}\, n_{kk'} = -\frac{\mathrm{i}}{\hbar}(\epsilon_{k'} - \epsilon_k) n_{kk'} - \frac{\mathrm{i}}{\hbar}\mathbf{E}(t)\cdot\sum_{l}\boldsymbol{\mu}_{lk} p_{lk'} + \frac{\mathrm{i}}{\hbar}\mathbf{E}(t)\cdot\sum_{l}\boldsymbol{\mu}^*_{lk'} p^*_{lk}, \tag{19}$$

$$\frac{\partial}{\partial t}\, n_{ll'} = -\frac{\mathrm{i}}{\hbar}(\epsilon_{l'} - \epsilon_l) n_{ll'} + \frac{\mathrm{i}}{\hbar}\mathbf{E}(t)\cdot\sum_{k}\boldsymbol{\mu}_{l'k} p_{lk} - \frac{\mathrm{i}}{\hbar}\mathbf{E}(t)\cdot\sum_{k}\boldsymbol{\mu}^*_{lk} p^*_{l'k} - \frac{\mathrm{i}}{\hbar}\mathbf{E}(t)\cdot\sum_{m}\boldsymbol{\mu}_{ml} p_{ml'} + \frac{\mathrm{i}}{\hbar}\mathbf{E}(t)\cdot\sum_{m}\boldsymbol{\mu}^*_{ml'} p^*_{ml}, \tag{20}$$

$$\frac{\partial}{\partial t}\, n_{mm'} = -\frac{\mathrm{i}}{\hbar}(\epsilon_{m'} - \epsilon_m) n_{mm'} + \frac{\mathrm{i}}{\hbar}\mathbf{E}(t)\cdot\sum_{l}\boldsymbol{\mu}_{m'l} p_{ml} - \frac{\mathrm{i}}{\hbar}\mathbf{E}(t)\cdot\sum_{l}\boldsymbol{\mu}^*_{ml} p^*_{m'l}. \tag{21}$$

These equations (16)–(21) are the OBE for the three-band multi-level system considered here. Their solutions for a specific incident field $\mathbf{E}(t)$ describe the dynamical evolution of the photoexcited system. The polarization $\tilde{p}_{mk}$—see equation (18)—yields the 2ω response which is measured in SHG. The electron populations measured in 2PPE are obtained from n_{mm}; see equation (21).

In the experimental investigations of time-resolved SHG which are discussed in sections 4 and 5, the signal is monitored in a diffraction direction and is at least of fourth order in the incident fields. Since the intensities of the incident fields reach only a few per cent of the saturation intensity, it is sufficient to analyse the experimental results by keeping only the lowest order terms (i.e. fourth order) that contribute to SHG. As a starting point, we assume that before the photoexcitation the system is in its ground state. This means that we start in zeroth order with $p^{(0)}_{lk} = p^{(0)}_{ml} = \tilde{p}^{(0)}_{mk} = n^{(0)}_{ll'} = n^{(0)}_{mm'} = 0$ and $n^{(0)}_{kk'} = \delta_{kk'}$, i.e., all coherences and the populations in excited bands vanish and only the valence band states (k-states) are populated. The resulting fourth-order equations describing time-resolved SHG are then obtained as

$$\frac{\partial}{\partial t}\, p^{(1)}_{lk} = -\frac{\mathrm{i}}{\hbar}(\epsilon_k - \epsilon_l)\, p^{(1)}_{lk} - \frac{\mathrm{i}}{\hbar}\mathbf{E}(t)\cdot\boldsymbol{\mu}^*_{lk}, \tag{22}$$

$$\frac{\partial}{\partial t}\, n^{(2)}_{ll'} = -\frac{\mathrm{i}}{\hbar}(\epsilon_{l'} - \epsilon_l) n^{(2)}_{ll'} + \frac{\mathrm{i}}{\hbar}\mathbf{E}(t)\cdot\sum_{k}\boldsymbol{\mu}_{l'k} p^{(1)}_{lk} - \frac{\mathrm{i}}{\hbar}\mathbf{E}(t)\cdot\sum_{k}\boldsymbol{\mu}^*_{lk} p^{(1)*}_{l'k}, \tag{23}$$

$$\frac{\partial}{\partial t}\, n^{(2)}_{kk'} = -\frac{\mathrm{i}}{\hbar}(\epsilon_{k'} - \epsilon_k) n^{(2)}_{kk'} - \frac{\mathrm{i}}{\hbar}\mathbf{E}(t)\cdot\sum_{l}\boldsymbol{\mu}_{lk} p^{(1)}_{lk'} + \frac{\mathrm{i}}{\hbar}\mathbf{E}(t)\cdot\sum_{l}\boldsymbol{\mu}^*_{lk'} p^{(1)*}_{lk}, \tag{24}$$

$$\frac{\partial}{\partial t}\,\tilde{p}^{(2)}_{mk} = -\frac{\mathrm{i}}{\hbar}(\epsilon_k - \epsilon_m)\,\tilde{p}^{(2)}_{mk} - \frac{\mathrm{i}}{\hbar}\mathbf{E}(t)\cdot\sum_{l'}\boldsymbol{\mu}^*_{ml'} p^{(1)}_{l'k}, \tag{25}$$

$$\frac{\partial}{\partial t}\, p^{(3)}_{lk} = -\frac{\mathrm{i}}{\hbar}(\epsilon_k - \epsilon_l)\, p^{(3)}_{lk} - \frac{\mathrm{i}}{\hbar}\mathbf{E}(t)\cdot\sum_{k'}\boldsymbol{\mu}^*_{lk'} n^{(2)}_{k'k} + \frac{\mathrm{i}}{\hbar}\mathbf{E}(t)\cdot\sum_{l'}\boldsymbol{\mu}^*_{l'k} n^{(2)}_{ll'} - \frac{\mathrm{i}}{\hbar}\mathbf{E}(t)\cdot\sum_{m'}\boldsymbol{\mu}_{m'l}\tilde{p}^{(2)}_{m'k}, \tag{26}$$

$$\frac{\partial}{\partial t}\, p^{(3)}_{ml} = -\frac{\mathrm{i}}{\hbar}(\epsilon_l - \epsilon_m)\, p^{(3)}_{ml} - \frac{\mathrm{i}}{\hbar}\mathbf{E}(t)\cdot\sum_{l'}\boldsymbol{\mu}^{*}_{ml'} n^{(2)}_{l'l} + \frac{\mathrm{i}}{\hbar}\mathbf{E}(t)\cdot\sum_{m'}\boldsymbol{\mu}^{*}_{m'l} n^{(2)}_{mm'} + \frac{\mathrm{i}}{\hbar}\mathbf{E}(t)\cdot\sum_{k'}\boldsymbol{\mu}_{lk'}\,\tilde{p}^{(2)}_{mk'} \tag{27}$$

$$\frac{\partial}{\partial t}\,\tilde{p}^{(4)}_{mk} = -\frac{\mathrm{i}}{\hbar}(\epsilon_k - \epsilon_m)\,\tilde{p}^{(4)}_{mk} - \frac{\mathrm{i}}{\hbar}\mathbf{E}(t)\cdot\sum_{l'}\boldsymbol{\mu}^{*}_{ml'} p^{(3)}_{l'k} + \frac{\mathrm{i}}{\hbar}\mathbf{E}(t)\cdot\sum_{l'}\boldsymbol{\mu}^{*}_{l'k} p^{(3)}_{ml'}. \tag{28}$$

The measured diffracted SHG signal is induced by the 2ω polarization:

$$\tilde{\mathbf{P}}^{(4)}_{2\omega} = \sum_{mk}(\tilde{\boldsymbol{\mu}}_{mk}\,\tilde{p}^{(4)}_{mk} + \tilde{\boldsymbol{\mu}}^{*}_{mk}(\tilde{p}^{(4)}_{mk})^{*}). \tag{29}$$

In order to describe the excitation with a sequence of incident laser pulses travelling in different directions $\mathbf{k}_i$ it is advantageous to perform a spatial Fourier expansion of the coupled equations [4, 48]. In this case, equations (22)–(28) have to be solved by keeping track of all interactions with the respective pulses yielding polarizations associated with the directions in which the signal is monitored.

At a phenomenological level, the decay of the experimentally measured transients can be described by supplementing equations (22)–(28) with dephasing and relaxation terms, which introduce decay of the interband and intraband coherences and relaxation of the populations. This procedure is used in sections 4 and 5 where we model measured SHG transients using sets of OBE for a few model systems.

3. Experimental set-up

The experiments presented below were conducted with a cavity-dumped Ti:sapphire laser system [49] that delivered trains of 800 nm pulses at repetition rates from 100 kHz to 2 MHz with pulse durations of 13 fs and pulse energies up to 50 nJ. A schematic diagram of the three-beam experimental set-up is displayed in figure 4. The p-polarized laser pulses were split with an intensity ratio of 3:7 in the two-beam pump–probe set-up, and of 2:1:1 in the three-beam geometry[1]. The beams were recombined on the sample at angles of 22° and 24° (two beams), and 19°, 22°, and 27° (three beams) with respect to the surface normal. The plane of incidence was normal to the $[2\bar{1}\bar{1}]$ direction of Si(111) and normal to [110] for Si(001). Typical excitation fluences were 100 μJ cm^{-2}, which is only about 2% of the saturation intensity for the transitions involved. The detection system was optimized for the simultaneous monitoring of two beams of 2ω radiation with wavelength around 400 nm at a rate ranging from 0.1 to 10^6 photons per second. The 5WM signal was detected with a photomultiplier without polarization selection. The relative time delays between the pulses were determined from the sum-frequency response of beams *a* and *b* and beams *b* and *c* which is symmetric with respect to delay times.

The experiments were carried out in an ultrahigh vacuum (UHV) chamber with a base pressure of 2×10^{-11} mbar. The base material used for the samples was single-crystal n-type phosphorus-doped silicon (Virginia Semiconductor) with specified resistivities between 6 and 12 Ω cm corresponding to a P donor density $\sim 5 \times 10^{14}$ cm^{-3}. The wafers with a thickness of 0.6 mm were single-side polished and oriented to within ±0.25° along the principal [111] or [001] axis. The samples were mounted on a liquid-nitrogen-cooled holder and could be heated resistively. The surfaces were prepared with single heating cycles peaking at ∼1300 K. The

[1] The effect of the polarization of the incident beams was studied systematically only in the case of the Si(111) two-beam set-up. The 5WM signal dropped by more than a factor of 20 and was below our detection limit when two orthogonally polarized input beams were used.

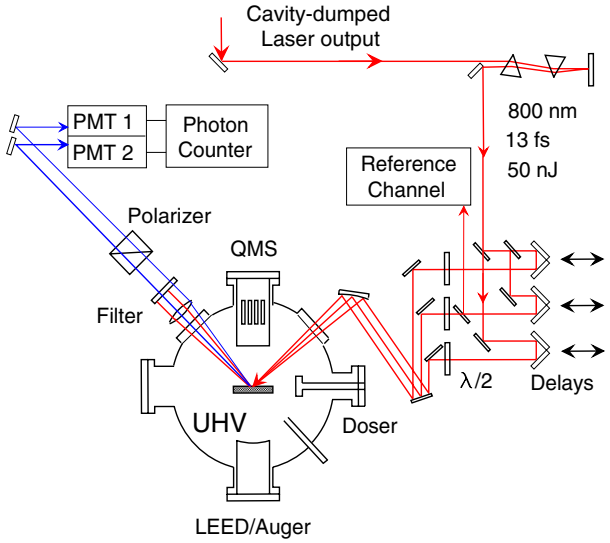

Figure 4. A schematic representation of the optical set-up for the SH diffraction experiment. After compression by two prisms, the pulses are split into two or three beams, which are focused onto the silicon surface in UHV. From the emerging bunch of reflected and diffracted beams from the surface, two SH rays are detected simultaneously and processed by a two-channel photon counter. Taken from [50].

quality of the surfaces was regularly inspected using LEED and Auger electron spectroscopy (AES). They showed sharp Si(001)-c(4 × 2) or Si(111)-(7 × 7) diffraction patterns and no traces of contamination. All measurements presented below were carried out at 80 K sample temperature.

4. Two-pulse second-harmonic generation at Si(111)7 × 7

Using laser pulses with photon energies of 1.55 eV one can excite, at the Si(111)7 × 7 surface, electrons from bulk valence bands near $\bar{\Gamma}$ into the dangling-bond derived surface band U_1 which lies above the Fermi level in this region of k-space. The dynamics of such excited electron populations $\bar{\Gamma}$ in the U_1 surface band has been investigated in [21] by monitoring the time-delay dependence of the SHG measured in a pump–probe experiment with pulse durations of 120 fs. It was found that the SHG intensity is decreased when the pump and probe arrive at the surface with no time delay. With increasing time delay, the SHG intensity recovers on a timescale of 215 fs which reflects the time for scattering of the excited electrons out of the optically coupled regions of k-space. In the language of the OBE one would model this process by a T_1 time which diminishes the electron population in the states photoexcited by the pump.

Further experiments presented in [21] showed results on the SFG and the self-diffracted SHG excited by two ultrashort pulses with duration shorter than 14 fs. The measured SFG cross-correlation is shown in figure 5(a). In the language of nonlinear optics the SFG is a second-order process which is described by

$$\mathbf{P}_{\mathrm{s}}^{(2)}(\mathbf{K}_{\mathrm{SF}}, 2\omega) = \chi_{\mathrm{s}}^{(2)} : \mathbf{E}_a(\mathbf{k}_a, \omega)\mathbf{E}_b(\mathbf{k}_b, \omega), \tag{30}$$

with

$$K_{\mathrm{SF},x} = k_{b,x} + k_{a,x}, \tag{31}$$

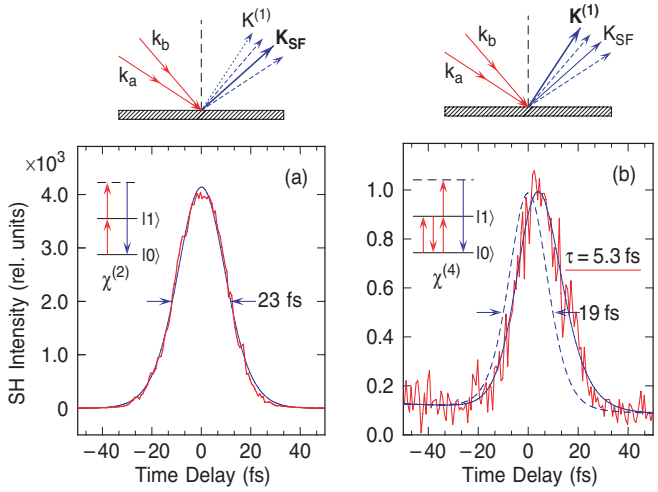

Figure 5. (a) SFG cross-correlation from two beams incident on a clean Si(111)7 × 7 surface under 22° and 24°. The solid line through the data indicates the calculated response of sech^2 pulses with a FWHM of less than 14 fs. (b) Self-diffracted SHG from two beams incident on a clean Si(111)7 × 7 surface under 22° and 24°. The dashed line through the data indicates the calculated response of sech^2 pulses with a FWHM of less than 14 fs. The shift and asymmetric broadening of the diffracted signal corresponds to a decay time of 5.2 fs. Taken from [21].

where $\mathbf{k}_a$ and $\mathbf{k}_b$ denote the directions of the two laser beams which are incident in the x–z plane (x denotes a direction parallel and z the direction perpendicular to the surface) and $\chi_s^{(2)}$ is the second-order nonlinear optical susceptibility. In centrosymmetric bulk materials this process is dipole forbidden. Therefore, the measured SFG is predominantly generated at the surface which is denoted by the subscript s in equation (30).

Since the SFG does not change on interchanging the two incident pulses, the measured transient in figure 5(a) is symmetric with respect to zero time delay. For both positive and negative time delays, it falls off rapidly showing a FWHM of only 23 fs. For incident pulses with an ideal sech^2 shape this width corresponds to a pulse duration of less than 14 fs on the sample.

The measured transient self-diffracted SHG is displayed in figure 5(b), where a positive time delay corresponds to a situation where pulse a is incident before pulse b. This process is described by

$$\mathbf{P}_s^{(4)}(\mathbf{K}_d^{(+1)}, 2\omega) = \chi_s^{(4)} : \mathbf{E}_a^*(\mathbf{k}_a, \omega)\mathbf{E}_b^3(\mathbf{k}_b, \omega), \tag{32}$$

with

$$K_{d,x}^{(+1)} = 3k_{b,x} - k_{a,x} = 2k_{b,x} + (k_{b,x} - k_{a,x}), \tag{33}$$

where $\chi_s^{(4)}$ is the fourth-order nonlinear optical susceptibility. One may view this 5WM process as SHG generated from a transient grating. In this scenario, the two time-delayed beams a and b produce a population grating at the surface which gives rise to a spatial modulation of the second-order nonlinear susceptibility, $\Delta\chi_s^{(2)}(x) = \Delta\chi_{s,0}^{(2)}\cos(k_G x)$, with $k_G = k_{b,x} - k_{a,x}$. A fraction of beam b then acts as a probe beam and is frequency doubled and Bragg scattered from the grating into the direction $\mathbf{K}_d^{(+1)}$. The detected SHG signal thus probes the modulation depth $\Delta\chi_{s,0}^{(2)}$ of the grating and therefore is proportional to the amount of polarization induced by beam a which is present when the time-delayed beam b arrives. Therefore, by measuring

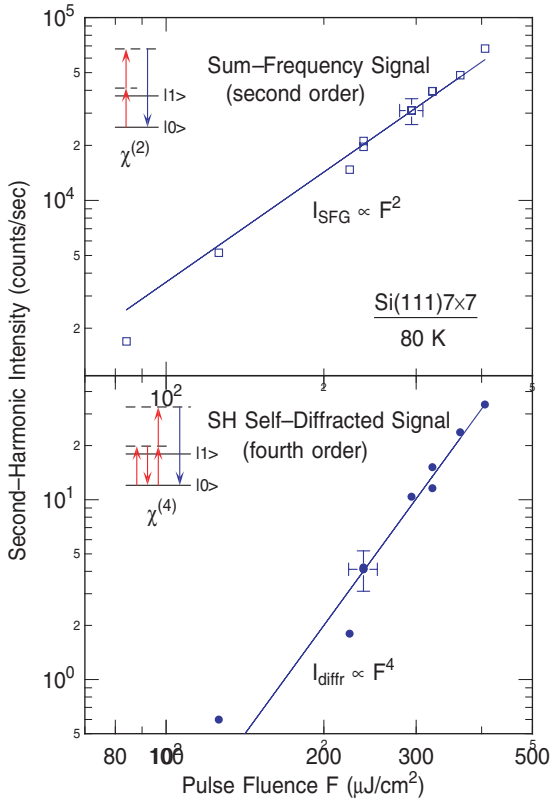

Figure 6. The SFG cross-correlation intensity (top) and self-diffracted SHG intensity (bottom) from a clean Si(111)7×7 surface as a function of the laser pulse fluence F. The lines fitted to the data are proportional to F^2 and F^4, respectively. After [21].

the time-delay dependence of the SHG one obtains information on the decay of the polarization induced by beam a.

The measured SHG in figure 5(b) shows a quick rise, a maximum at a time delay of about 5 fs, and then decays very rapidly with increasing time delay. This transient behaviour implies that the polarization generated by pulse a has to decay very rapidly on a timescale comparable to the duration of the incident ultrashort laser pulses.

The fluence dependence of the SFG and the SHG signals—see figure 6—verifies the nonlinear nature of the measurements. In agreement with lowest order perturbation theory with respect to the light–matter coupling, the SFG signal scales with the square of the fluence and the SHG signal with the fourth power of the fluence. Hence, we can be sure that the experiments have been performed with pulse intensities which are much smaller than the saturation intensities.

The simplest modelling of the measured SHG transients shown in figure 5(b) would be done considering only a single three-level system. However, since the experiments have been performed on a solid-state system which is characterized by a band structure of the surface and bulk bands, one has to include a distribution of the transition energies. This is particularly important since the ultrashort laser pulses cover a very wide spectrum of transition energies and we do not expect any discrete (e.g., excitonic) resonances to dominate in the signals. The presence of different transition energies can, however, be due to different physical processes and thus can be modelled in different ways. In the following, we concentrate on the transition from the initially occupied valence states to the intermediate band which are induced by pulse a, since this polarization is the most important quantity determining measured SHG transients.

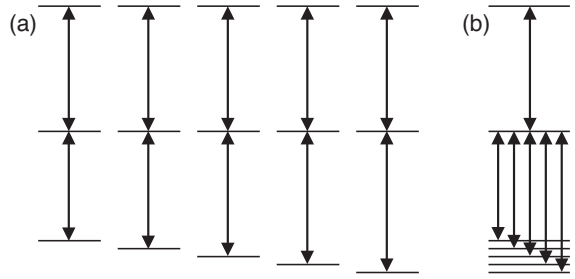

Figure 7. Model systems used for describing the time-resolved SHG. (a) The inhomogeneous model describing the dispersion of the valence band in k-space. (b) The homogeneous model which considers a continuum of projected bulk valence band states for a particular k-state.

Due to the dispersion of band-to-band transitions and the fact that the optical transitions are diagonal in k-space, one could model the SHG by considering an inhomogeneous distribution of the three-level system, where each of the systems characterizes a particular point in k-space. Such an ensemble of systems—see figure 7(a)—is referred to as the *inhomogeneous* model. As the other extreme, one could think that the response is mainly due to a particular k-state and that at this state the folded bulk valence bands provide a continuum of energies which are optically coupled to the same excited state. This system—see figure 7(b)—is referred to as the *homogeneous* model. In reality, one probably has to take into account both homogeneous and inhomogeneous broadening where their relative importance is determined by the dependences on energy and k of the matrix elements which govern the optical response. Since at present no such complete model exists, we analyse here the two extreme cases in order to highlight their principle differences when applied to time-resolved SHG.

The calculated self-diffracted SHG for the inhomogeneous and the homogeneous models are shown in figure 8. For both models, the widths of the continuum in the valence bands were chosen to exceed the spectral width of the incident pulses and the dipole matrix elements were kept constant. Analysing 4WM for the inhomogeneous model one would get a photon echo in the time-resolved signal. Therefore, without dephasing, i.e., for $T_2 = \infty$, the time-integrated 4WM signal would rise with increasing time delay and reach its maximum when the delay equals the temporal width of the photon echo. Note that for our model, the temporal width of the echo is determined by the duration of the laser pulses, since the continuum considered is very broad. This behaviour of the 4WM qualitatively explains the results obtained for the 5WM process, i.e., the diffracted SHG intensity. For $T_2 = \infty$—see the dashed curve in figure 8(a)—the signal rises with increasing time delay and reaches its maximum at a delay of about 50 fs. This maximum at a time delay bigger than the duration of the pulses is a consequence of the nonlinear convolution of the incident pulses which results in a temporal broadening of the signal. For shorter dephasing times, the maxima of the SHG signal shift to smaller delays; see the dotted and solid curves in figure 8(a). Comparing the calculation to the experimental data, figure 5(b), we would conclude from this model that the dephasing time has to be of the order of 10 fs.

However, if one alternatively uses the homogeneous model, one arrives at a completely different picture. As shown in figure 8(b), within this model the SHG transients are basically independent of the dephasing time considered. This is due to the fact that the decay of the interband polarization in such a model, where the transitions induced by pulse a share a common state, is irreversible [48, 51]. Thus, in this case we do not get a photon echo but just a rapid decay which for a broad continuum of transitions occurs on a timescale comparable to the duration of the laser pulses. Therefore, if the homogeneous model were to be the correct

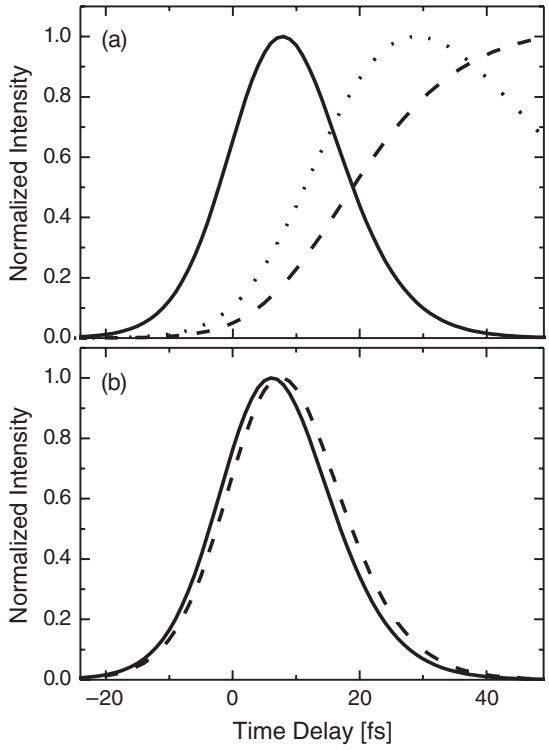

Figure 8. Calculated self-diffracted SHG induced by two laser beams. (a) Numerical results obtained for the inhomogeneous model using $T_2 = 3$ fs (solid), 100 fs (dotted), and ∞ (dashed). (b) Numerical results obtained for the homogeneous model using $T_2 = 3$ fs (solid) and ∞ (dashed).

description, the measured SHG transients would not allow for any conclusions on the dephasing time, since the internal dynamics of the system would be responsible for the rapid decay of the signal.

These two extreme examples highlight problems one may face when describing optical transients at the level of OBE with phenomenological inputs. If one does not have beforehand information about the nature of the underlying states and their most important optical transitions, it may often not be possible to give a conclusive description of experimental results since very different models can lead to very similar signatures. This demonstrates furthermore that it is highly desirable to analyse such nonlinear optical experiments using microscopic theory, such as extensions of the SBE presented in section 2.1.

5. Three-pulse second-harmonic generation at Si(001)-c(4 × 2)

In this section we discuss results on time-resolved SHG obtained by exciting the Si(001)-c(4 × 2) surface with three ultrashort laser pulses of frequency ω; see [22]. The measured diffracted 2ω radiation is generated by nonlinear optical interactions at the Si(001)-c(4 × 2) surface. The three beams with wavevectors $\mathbf{k}_a$, $\mathbf{k}_b$, and $\mathbf{k}_c$ are incident in the x–z plane. The SHG signal is detected in a reflection geometry. To lowest order in the fields, the SHG source is the fourth-order polarization

$$\mathbf{P}_{\mathrm{s}}^{(4)}(\mathbf{K}_d^{(+1)}, 2\omega) = \chi_{\mathrm{s}}^{(4)} : \mathbf{E}_a^*(\mathbf{k}_a, \omega)\mathbf{E}_b(\mathbf{k}_b, \omega)\mathbf{E}_c^2(\mathbf{k}_c, \omega), \tag{34}$$

with

$$K_{d,x}^{(+1)} = 2k_{c,x} + k_{b,x} - k_{a,x}, \tag{35}$$

where $\chi_{\mathrm{s}}^{(4)}$ is the fourth-order nonlinear optical susceptibility.

Considering that pulse c arrives last, one may view the 5WM process described by equation (34) as SHG generated from a transient grating. In this scenario, the two pump beams a and b produce a population grating. The time-delayed probe beam c is frequency doubled and Bragg scattered from the grating into the direction $\mathbf{K}_d^{(+1)}$. The detected 2ω signal thus probes the modulation depth $\Delta\chi_{s,0}^{(2)}$ of the grating as a function of the delay of beam c. The SHG signal therefore contains information about carrier relaxation and carrier diffusion at the surface. This simplified picture of the 5WM process is valid only for delays of beam c that are considerably longer than the durations of the exciting laser pulses and the dephasing times of the system. In general, several terms arising from the coherent interaction of the three beams contribute to the 5WM signal.

By varying the time ordering of the pulses the versatile three-beam technique can also be used to study the temporal evolution of photoexcited one- and two-photon coherences. For example, when the delay between beams a and b is varied, the SHG signal contains information about the decay of optical polarizations, as is the case for the self-diffracted SHG signal analysed in section 4. Information on the dynamics of higher order optical coherences can be gained if beam c arrives first, which generates in second order a 2ω polarization. By varying the delays with respect to beams a and b one can measure the dynamics of this two-photon polarization.

Representative data showing the dependence of the SHG intensity as a function of the delay time τ_{ab} between the (pump) beams a and b are shown in figure 9(b). The different curves correspond to a different delay time τ_{bc} of (probe) beam c with respect to beam b. The delay times are defined with respect to the time of incidence of pulse b; i.e., a pulse sequence a, b, c corresponds to $\tau_{ab} < 0$ and $\tau_{bc} > 0$. So the definition of the sign of the delay is opposite to that used in figure 5(b).

As shown in figure 9(b), the 2ω response is for all delays τ_{bc} sharply peaked close to $\tau_{ab} = 0$ and is an almost symmetric function of τ_{ab}. The FWHM of 23 fs is similar to that of the SFG induced by beams a and b. The FWHM of the SFG is determined by the cross-correlation of the two laser beams and the decay of the surface polarization generated. As a function of τ_{ab} the results of the three-beam SHG experiment are similar to those for the self-diffraction two-beam SHG data reported for Si(111)-7 $\times$ 7 [21]; see figure 5(b). As discussed in section 4, it is therefore not possible to decide from the experimental data alone whether the fast decay is a result of dephasing due to rapid scattering processes or has its origin in the destructive interference of a continuum of transition frequencies. In any case, the rapid decay of the SHG intensity as a function of τ_{ab} considerably simplifies the analysis of the temporal response of the 5WM signal as a function of delay time τ_{bc}. For $\tau_{bc} > 38$ fs (sum of pulse width and sum-frequency signal) it is possible to interpret the measured response as SHG from a transient population grating as described above.

We concentrate in the following on the variation of the peak intensity with the delay of the probe beam c. This dynamics is displayed in figure 10 where the peak maxima from the data of figure 9(b) and from similar measurements are plotted as a function of τ_{bc}. Surprisingly, in this case the intensity does not show just a simple rise followed by a subsequent decay, but instead the measured transient peaks at two temporal positions. After showing a sharp maximum around $\tau_{bc} = 0$, the intensity goes through a minimum, then reaches its absolute maximum at a delay of $\sim$100 fs, before it subsequently decays to zero on a timescale of 500 fs.

Whereas the sharp maximum at $\tau_{bc} = 0$ can be understood simply as the result of the coherent interaction of all three beams, the occurrence of a maximum, long after the two pump beams a and b are over, is unexpected. In a usual transient grating experiment, one expects the grating modulation to reach its maximum immediately after the incidence of the excitation pulses a and b. Thus, one would expect the maximum intensity to be observed for

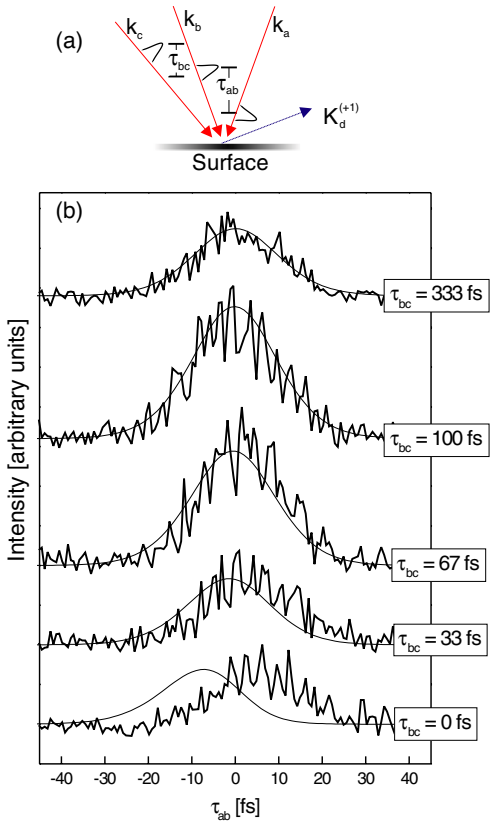

Figure 9. (a) The geometry of the 5WM experiment using three temporally delayed incident beams a, b, and c. The SH intensity is measured in the reflected direction $\mathbf{K}_d^{(+1)}$. (b) Time-integrated SH intensity as a function of τ_{ab} for varying τ_{bc}. The thick solid curves are the measured transients and the thin curves display the results of the model calculations. Taken from [22].

small positive τ_{bc} which is close to the duration of the pulses. Considering a short population relaxation time T_1, the temporal position of this maximum should be shifted even closer to zero delay since in this case excitation and decay compete with each other. A shift in the opposite direction, i.e., towards longer positive delays, as observed in figure 10, can only be understood by considering some kind of process of transfer between the generation of the grating and the probe of its properties.

Since due to the overwhelming complexity of the interaction processes among surface and bulk states a fully microscopic description for the time-resolved SHG at surfaces is currently not available, we use a description which is based on the OBE and phenomenologically incorporates known facts for the system to analyse the 5WM experiment. With the photon energies of 1.55 eV delivered by our laser system, SHG from silicon is resonantly enhanced by dangling-bond derived surface states (1ω resonance) and by surface-distorted bulk states (2ω resonance near the E_1 transition of bulk Si) [52–55]. In the case of Si(001), the dangling bonds are the D_{up} and D_{down} states of the asymmetric dimers. Considering the band structure—see figure 11(a)—one finds that resonant optical transitions from D_{up} to D_{down} are possible between the $\bar{\Gamma}$ and $\bar{J}'$ points of the surface Brillouin zone. Since in this region of k-space the electrons are photoexcited well above the bottom of the D_{down} band, it is reasonable to assume that they

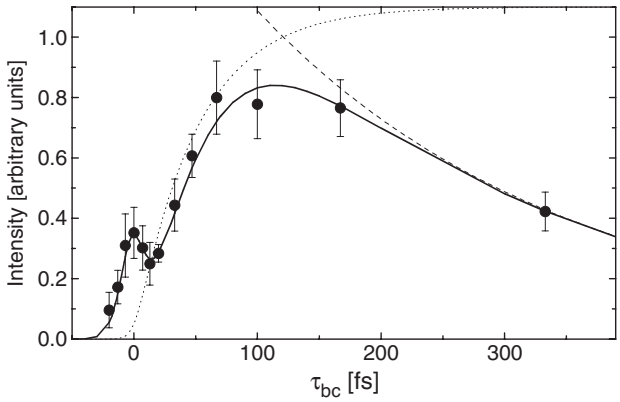

Figure 10. SH peak intensity, i.e., the maximum of the 5WM signal for varying τ_{ab} but fixed τ_{bc}, as a function of τ_{bc}. The circles (with error bars) are the experimental results and the solid curve displays the transient obtained from the model calculations. The dashed curve denotes the long time limit, where the intensity is dominated by T_1 processes and thus proportional to $(\exp(-t/T_1))^2$ with $T_1 = 500$ fs. The dotted curve displays the population at the lower one-photon resonance $|1'\rangle$ of system S′ (see figure 11) induced by a transfer time of $T_{\text{trans}} = 50$ fs neglecting T_1 processes. Taken from [22].

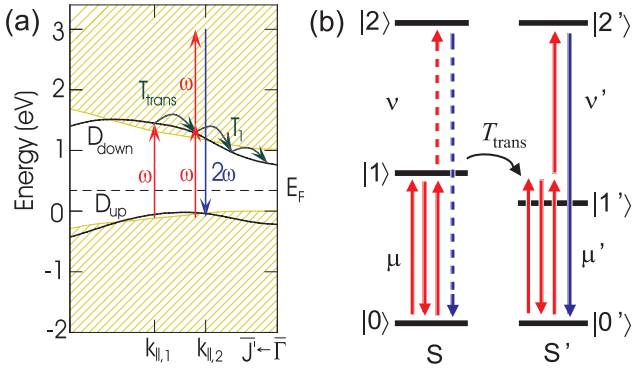

Figure 11. (a) The band structure of Si(001)-c(4 × 2), after [58]. (b) The two coupled three-level systems S and S′ used in the numerical model calculations. Electronic relaxation from $|1\rangle$ and $|1'\rangle$ is modelled by a transfer time T_{trans}. The energy differences between $|0\rangle$ and $|2\rangle$ and $|0'\rangle$ and $|2'\rangle$ both coincide with twice the frequency of the incident beams. Taken from [22].

will rapidly scatter towards lower energies and probably accumulate close to $\bar{\Gamma}$ and/or $\bar{J}'$. This rapid relaxation process could be due to the emission of phonons associated with a flipping of the excited dimers and may be accelerated by simultaneous Coulomb scattering processes.

Whereas in a standard 4WM experiment the excitation grating generated by beams *a* and *b* would be probed by beam *c* at the same position in *k*-space, this is generally not the case in a 5WM experiment. This difference is due to the fact that the generation of the diffracted SH signal involves optical transitions at both ω and 2ω induced by the probe, which are governed by different matrix elements to those of the pump. In particular, in a situation where 2ω is close to a resonance, as is the case in our experiment, it is possible to monitor the excitation grating at energies and momenta substantially different from those initially created by the two pump beams. Consequently, the temporal response of the diffracted signal reflects scattering both *in* and *out* of the optically probed region in *k*-space. We would like to emphasize that, as matrix

elements involving surface transitions are generally not well known, it does not matter for our interpretation whether the electrons created in the D_{down} band originate from the D_{up} band or from bulk-like states. Furthermore, we would like to mention that the proposed excitation and scattering process is in agreement with 2PPE measurements which have recently been performed by Weinelt *et al* [16].

To substantiate the interpretation given above, we numerically solve OBE for a model consisting of two coupled three-level systems S and S′; see figure 11(b). As outlined in section 2.2, the 5WM signal is calculated up to fourth order in the fields by numerically solving the OBE for the relevant interband and intraband coherences and the populations taking into account the finite duration of the exciting pulses. Dephasing and population relaxation are described phenomenologically using time constants T_2 and T_1, respectively.

The calculated 5WM signals as a function of τ_{ab} are shown by the thin curves in figure 9(b). If τ_{bc} is not too small, i.e., when the 5WM signal can be interpreted as a diffraction off a transient grating, the numerical results concerning the dependence on both τ_{ab} and τ_{bc} are in good agreement with experiment. For very small $|\tau_{bc}|$ of the order of a few pulse widths, the numerical transients are shifted as a function of τ_{ab} relative to experiment. The origin of this temporal shift could be that our simple model does not include the continuum of off-resonant transitions, three-photon resonances, and many-body interactions among the photoexcitations, which are known to lead to signals for positive τ_{ab} in 4WM experiments [56]. It should be noted that the sign of τ in [56] is reversed with respect to our definition of τ_{ab}. Since the main experimental feature that we want to investigate here is the delayed maximum observed in figure 10, the temporal shift between solid curves in figure 9(b) for very small $|\tau_{bc}|$ is of no importance for the present analysis.

By calculating the SHG intensity as a function of τ_{bc} for ensembles of uncoupled three-level systems, i.e., an inhomogeneous model, it is not possible to reproduce the delayed maximum of the experimental data of figure 10. As argued above, the numerical calculations (not shown in the figure) show that for this case the maximum of the SHG intensity appears always at small positive τ_{bc}. The delayed maximum can, however, be reproduced by considering a coupling between the two three-level systems S and S′ by a transfer process which models population relaxation from level $|1\rangle$ to level $|1'\rangle$. In more detail, we assume that for positive τ_{bc}, beams a and b resonantly create a strong population grating at $|1\rangle$ and a much weaker off-resonant excitation at $|1'\rangle$. With increasing time, the population of $|1\rangle$ is relaxing to $|1'\rangle$. This process is modelled by a transfer time of $T_{\text{trans}} = 50$ fs. For bulk silicon, 4WM experiments with 100 fs beams have revealed ultrafast dynamics on a timescale of ∼10 fs up to several 100 fs [23, 57]. 2PPE experiments with 150 fs beams showed extremely rapid thermalization and cooling of photoexcited electrons (<100 fs) [59, 60]. Therefore, the rapid timescale observed here with our short 13 fs beams does not seem to be unreasonable. The experimental observation that the delayed maximum is bigger than the initial one is reproduced by enhancing the transition matrix elements for the system S′ in comparison to S in figure 11(b). This reduced model can be viewed as representing the most important transitions in the band structure. The system S corresponds to the value $k_{\parallel,1}$ between $\bar{\Gamma}$ and $\bar{J}'$. In this region resonant single-photon transitions to the D_{down} band, which is represented by $|1\rangle$, are expected. The system S′ is situated at $k_{\parallel,2}$, closer to the minimum of the D_{down} band, e.g., closer to the $\bar{\Gamma}$ point.

The results of our numerical calculations concerning the dependence of the SHG peak intensity as a function of τ_{bc} are shown by the solid curve in figure 10. Clearly, the experimental data are reproduced very well by the model considered. The long time limit is dominated by T_1 processes; see the dashed curve in figure 10. The slow rise of the signal has its origin in the population transfer to $|1'\rangle$; see the dotted curve. Qualitatively, the delayed maximum can be described by considering the product of the dashed and dotted curves.

In addition to the rapid scattering processes in the D_{down} band discussed here, recent 2PPE studies by Tanaka and Tanimura [15] and by Weinelt *et al* [16] have reported a long lived component of the D_{down} population at the $\bar{\Gamma}$ point. It has been suggested that this component arises from scattering of bulk electrons from the conduction band minimum into the D_{down} band and that the decay time of ∼200 ps reflects the lifetime of the bulk electrons [16]. In our experiment we observe neither a signature of this bulk–surface scattering process nor one of the faster 5 ps decay of the population at the $\bar{\Gamma}$ point of the D_{down} band which has been attributed to exciton formation [16].

This difference between the 2PPE and 5WM experiments is consistent with the microscopic interpretation of the 5WM processes given above. The 2PPE experiments used a pump photon energy similar to the fundamental photon energy of our 5WM set-up. Thus the two experiments excite a similar region of the surface Brillouin zone. However, the 5WM signal from Si(001) originates predominantly from a region in k-space that is close to the point where the D_{down} band is resonantly excited (compare figure 11) whereas the long lived 2PPE signals originate from the $\bar{\Gamma}$ point. According to Weinelt *et al* [16], electrons at $k_{\parallel} = 0$ have already lost 350 meV compared to their energy at $k_{\parallel} = 0.11$ Å^{-1} where a resonant excitation between the D_{up} and D_{down} states is possible. It is very unlikely that any region in k-space with such a large detuning of the $|0'\rangle \rightarrow |1'\rangle$ transition can significantly contribute to the 5WM response when near-resonant transitions are possible for other values of k. Under the present conditions, the 5WM experiment thus selectively probes intra-band scattering close to the region of excitation and it is not sensitive to electron dynamics at the band minimum.

As a concluding remark concerning the comparison of time-resolved 5WM with other ultrafast probes that have been used to investigate electron dynamics at silicon surfaces and interfaces, we would like to stress its interface specificity as an even-order nonlinear optical process. Resonant excitation of surface states with a photon energy below the direct band gap of the bulk will generally only lead to a much weaker density of excited carriers in the bulk than at the surface. These bulk carriers can nevertheless contribute significantly to the response of third-order optical techniques such as conventional transient grating experiments [23, 24] or pump–probe reflectivity experiments [61] with a probing depth of $\lambda/4\pi n \sim 200$ Å, i.e., ∼100 atomic layers. Moderate bulk carrier densities will, however, not influence the 5WM response since its sensitivity is based on a symmetry break at the surface which occurs in the topmost 1–3 atomic layers. On an oxidized surface, e.g., pump pulses of a fluence similar to the one used in the present experiment give rise to transient reflectivity changes with a recovery time of the order of 100 ps [61]. When we quench the surface dangling bonds via oxygen adsorption the 5WM signal vanishes below the detection limit [50].

In 2PPE experiments, the excitation of long lived bulk states can severely influence the spectra in an indirect way, by changing the band bending at the surface and thus shifting the surface bands with respect to the Fermi level. Depending on the doping of the sample, the repetition rate of the laser, the concentration and transport characteristics of the bulk carriers, and other effects, this shift of the reference level for photoelectron spectroscopy can lead to shifts and/or broadening of 2PPE peaks [6]. As an all-optical technique the 5WM approach does not suffer from such photovoltage-induced effects. The technique can therefore be applied equally well to surfaces and interfaces with flat bands and significant band bending. Furthermore, it is also possible to apply it under conditions of high excitation densities where photoelectron spectra suffer from space charge effects [62].

6. Summary

In summary, experimental results on the temporal dynamics of the diffracted second-harmonic intensity at silicon surfaces have been presented and discussed. At the Si(111)7 × 7 surface,

the self-diffracted signal induced by two ultrashort laser beams shows a rapid decay on a timescale comparable to the duration of the incident pulses of less than 15 fs. It has been demonstrated by numerical solutions of the optical Bloch equations for model systems that it cannot be decided from the experimental data alone whether this dynamics is due to the decay of individual uncoupled polarizations, i.e., a T_2 process, or is the result of the destructive interference of a system of coupled polarizations. To distinguish these processes, a microscopic modelling of the second-harmonic generation including all optical matrix elements and further relevant interaction processes is required.

The Si(001)c(4 × 2) surface has been studied using a five-wave-mixing set-up which measures the diffracted second-harmonic intensity induced by three femtosecond laser beams. It has been demonstrated that by varying individual time delays between the pulses, this technique can not only be used to investigate the dynamics of one-photon transitions, but also allows one to monitor the temporal evolution of populations. With the support of model calculations based on optical Bloch equations, the observed ultrafast response as a function of a particular delay can be assigned to scattering of the excited electrons within the D_{down} surface band on timescales of 50–500 fs.

In the future, similar five-wave-mixing experiments using tunable laser pulses will allow us to investigate the processes discussed here in more detail, analyse the ultrafast optically induced dynamics at other surfaces, and access the largely unexplored electron dynamics of buried semiconductor interfaces. Theoretically, more microscopic approaches will be developed to gain a better quantitative understanding of the material dynamics which is responsible for the dynamics of nonlinear optical excitations at surfaces and interfaces.

Acknowledgments

We wish to acknowledge fruitful discussions with M Rohlfing and C Voelkmann. M Rohlfing also provided the quasiparticle wavefunctions used for evaluating the matrix elements that enter the semiconductor Bloch equations and C Voelkmann performed the wave-mixing experiments. This work was funded by the Deutsche Forschungsgemeinschaft (DFG), partly through HO2295/3, the Max-Planck Research programme of the Humboldt and Max-Planck societies, and by the Centre for Optodynamics, Philipps University, Marburg. We thank the John von Neumann Institut für Computing (NIC), Forschungszentrum Jülich, Germany, for grants for extended CPU time on their supercomputer systems. TM thanks the DFG for support via a Heisenberg fellowship (ME 1916/1-1).

References

[1] Chemla D S and Shah J 2001 *Nature* **411** 549
[2] Tsen K T (ed) 2001 Ultrafast physical processes in semiconductors *Semiconductors and Semimetals* vol 67 (San Diego, CA: Academic)
[3] Schäfer W and Wegener M 2002 *Semiconductor Optics and Transport Phenomena* (Berlin: Springer)
[4] Haug H and Koch S W 2004 *Quantum Theory of the Optical and Electronic Properties of Semiconductors* 4th edn (Singapore: World Scientific)
[5] Bokor J 1989 *Science* **246** 1130
[6] Haight R 1995 *Surf. Sci. Rep.* **21** 275
[7] Petek H and Ogawa S 1997 *Prog. Surf. Sci.* **56** 239
[8] Höfer U, Shumay I L, Reuss C, Thomann U, Wallauer W and Fauster T 1997 *Science* **277** 1480
[9] Berthold W, Höfer U, Feulner P, Chulkov E V, Silkin V M and Echenique P M 2002 *Phys. Rev. Lett.* **88** 056805
[10] Boger K, Weinelt M and Fauster T 2004 *Phys. Rev. Lett.* **92** 126803
[11] Ge N H, Wong C M, Lingle R L, McNeill J D, Gaffney K J and Harris C B 1998 *Science* **279** 202
[12] Gahl C, Bovensiepen U, Frischkorn C and Wolf M 2002 *Phys. Rev. Lett.* **89** 107402
[13] Bauer M, Pawlik S and Aeschlimann M 1999 *Phys. Rev.* B **60** 5016

[14] Petek H, Weida M J, Nagano H and Ogawa S 2000 *Science* **288** 1402
[15] Tanaka S and Tanimura K 2003 *Surf. Sci.* **529** L251
[16] Weinelt M, Kutschera M, Fauster T and Rohlfing M 2004 *Phys. Rev. Lett.* **92** 126801
[17] Shen Y R 1989 *Annu. Rev. Phys. Chem.* **40** 327
[18] Reider G A and Heinz T F 1995 *Photonic Probes of Surfaces* ed P Halevi (Amsterdam: North-Holland) pp 3–66
[19] Tom H W K, Aumiller G D and Brito-Cruz C H 1988 *Phys. Rev. Lett.* **60** 1438
[20] Hohlfeld J, Wellershoff S-S, Güdde J, Conrad U, Jähnke V and Matthias E 2000 *Chem. Phys.* **251** 235
[21] Voelkmann C, Mauerer M, Berthold W and Höfer U 1999 *Phys. Status Solidi* a **175** 169
[22] Voelkmann C, Reichelt M, Meier T, Koch S W and Höfer U 2004 *Phys. Rev. Lett.* **92** 127405
[23] Sjodin T, Petek H and Dai H L 1998 *Phys. Rev. Lett.* **81** 5664
[24] Sjodin T, Li C M, Petek H and Dai H L 2000 *Chem. Phys.* **251** 205
[25] Reichelt M, Meier T, Koch S W and Rohlfing M 2003 *Phys. Rev.* B **68** 045330
[26] Reichelt M, Meier T, Koch S W and Rohlfing M 2003 *Phys. Status Solidi* b **238** 525
[27] Hybertsen M S and Louie S G 1985 *Phys. Rev. Lett.* **55** 1418
[28] Godby R W, Schlüter M and Sham L J 1986 *Phys. Rev. Lett.* **56** 2415
[29] Rohlfing M and Louie S G 1999 *Phys. Rev. Lett.* **83** 856
[30] Allen L and Eberly J H 1975 *Optical Resonance and Two-Level Atoms* (New York: Wiley)
[31] Mayer E J *et al* 1994 *Phys. Rev.* B **50** 14730
[32] Mayer E J *et al* 1995 *Phys. Rev.* B **51** 10909
[33] Bott K *et al* 1996 *J. Opt. Soc. Am.* B **13** 1026
[34] Reichelt M, Sieh C, Meier T and Koch S W 2000 *Phys. Status Solidi* b **221** 249
[35] Stroucken T, Knorr A, Thomas P and Koch S W 1996 *Phys. Rev.* B **53** 2026
[36] Bànyai L, Tran Thoai D B, Reitsamer E, Haug H, Steinbach D, Wehner M U, Wegener M, Marschner T and Stolz W 1995 *Phys. Rev. Lett.* **75** 2188
[37] Jahnke F *et al* 1996 *Phys. Rev. Lett.* **77** 5257
[38] Koch S W, Meier T, Jahnke F and Thomas P 2000 *Appl. Phys.* A **71** 511
[39] Weiser S, Meier T, Möbius J, Euteneuer A, Mayer E J, Stolz W, Hofmann M, Rühle W W, Thomas P and Koch S W 2000 *Phys. Rev.* B **61** 13088
[40] Schmitt-Rink S, Chemla D S and Haug H 1998 *Phys. Rev.* B **37** 941
[41] Lindberg M and Koch S W 1998 *Phys. Rev.* B **38** 3342
[42] Sieh C, Meier T, Jahnke F, Knorr A, Koch S W, Brick P, Hübner M, Ell C, Prineas J, Khitrova G and Gibbs H M 1999 *Phys. Rev. Lett.* **82** 3112
[43] Sieh C, Meier T, Knorr A, Jahnke F, Thomas P and Koch S W 1999 *Eur. Phys. J.* B **11** 407
[44] Brick P, Ell C, Khitrova G, Gibbs H M, Meier T, Sieh C and Koch S W 2001 *Phys. Rev.* B **64** 075323
[45] Koch S W, Kira M and Meier T 2001 *J. Opt. B: Quantum Semiclass. Opt.* **3** R29
[46] Chiaradia P, Cricenti A, Selci S and Chiarotti G 1984 *Phys. Rev. Lett.* **52** 1145
[47] Pandey K C 1982 *Phys. Rev. Lett.* **49** 223
[48] Meier T, Schulze A, Thomas P, Vaupel H and Maschke K 1995 *Phys. Rev.* B **51** 13977
[49] Pshenichnikov M S, de Boeij W P and Wiersma D A 1994 *Opt. Lett.* **19** 572
[50] Voelkmann C 2001 *Dissertation* Technische Universität München, Germany
[51] Yeh J J and Eberly J H 1980 *Phys. Rev.* A **22** 1124
[52] Daum W, Krause H-J, Reichel U and Ibach H 1993 *Phys. Rev. Lett.* **71** 1234
[53] Höfer U 1996 *Appl. Phys.* A **63** 533
[54] Dadap J I, Xu Z, Hu X F, Downer M C, Russell N M, Ekerdt J G and Aktsipetrov O A 1997 *Phys. Rev.* B **56** 13367
[55] Mendoza B S, Palummo M, Onida G and Del Sole R 2001 *Phys. Rev.* B **63** 205406
[56] Leo K, Wegener M, Shah J, Chemla D S, Göbel E O, Damen T C, Schmitt-Rink S and Schäfer W 1990 *Phys. Rev. Lett.* **65** 1340
[57] Buhleier R, Lüpke G, Marowsky G, Gogolak Z and Kuhl J 1994 *Phys. Rev.* B **50** 2425
[58] Pollmann J, Krüger P, Rohlfing M, Sabisch M and Vogel V 1996 *Appl. Surf. Sci.* **104/105** 1
[59] Goldman J R and Prybyla J A 1994 *Phys. Rev. Lett.* **72** 1364
[60] Jeong S, Zacharias H and Bokor J 1996 *Phys. Rev.* B **54** R17300
[61] Sabbah A J and Riffe D M 2002 *Phys. Rev.* B **66** 165217
[62] Mauerer M, Berthold W, Shumay I L and Höfer U 2004 *Phys. Rev.* B submitted